

Overcoming the Distance Estimation Bottleneck in Camera Trap Distance Sampling

Timm Haucke^{*1}, Hjalmar S. Kühl², Jacqueline Hoyer², and Volker Steinhage^{†1}

¹University of Bonn, Institute of Computer Science IV,
Friedrich-Hirzebruch-Allee 8, Bonn 53115, Germany

²German Centre for Integrative Biodiversity Research (iDiv)
Halle-Jena-Leipzig, Puschstrasse 4, 04103 Leipzig, Germany

Biodiversity crisis is still accelerating. Estimating animal abundance is of critical importance to assess, for example, the consequences of land-use change and invasive species on species composition, or the effectiveness of conservation interventions. Camera trap distance sampling (CTDS) is a recently developed monitoring method providing reliable estimates of wildlife population density and abundance. However, in current applications of CTDS, the required camera-to-animal distance measurements are derived by laborious, manual and subjective estimation methods. To overcome this distance estimation bottleneck in CTDS, this study proposes a completely automatized workflow utilizing state-of-the-art methods of image processing and pattern recognition.

Keywords: Animal density, animal abundance, camera trapping, camera trap distance sampling, automated distance estimation, image processing, pattern recognition

*haucke@cs.uni-bonn.de

†steinhage@cs.uni-bonn.de

1. Introduction

The dramatic decrease in biodiversity and wild animal populations require the accurate and large-scale monitoring of wildlife. Camera trap distance sampling (CTDS) (Howe et al., 2017) is a proven approach to estimate animal densities and abundances with camera trap imagery from a limited set of locations (point transects). CTDS has been successfully applied to, for example, Maxwell’s duiker (*Philantomba maxwellii*), i.e., small antelopes in western Africa (Howe et al., 2017), western chimpanzees (*Pan troglodytes verus*) in Taï National Park, Côte d’Ivoire (Cappelle et al., 2019), to a diverse vertebrate community in Salonga National Park, situated in the Cuvette Centrale, DRC (Bessone et al., 2020) and to alpine marmots (*Marmota marmota*) in Stelvio National Park, Italy (Corlatti et al., 2020).

1.1. Problem statement

However, CTDS requires the observation distances, i.e., the distances from the respective camera trap to the observed animals. Currently, there are two methods for such distance measurements based on camera trap imagery:

- Visual estimation by reference images: Following Howe et al. (2017), distances between the camera trap’s lens and the midpoint of each detected animal are estimated by an operator by comparing animal locations in the given observation video to reference images taken at known distances from camera during camera installation (e.g., from 1 to 12 m).
- On-site distance measurement: distances between the camera trap’s location and each previously observed animal are measured by an operator in the field, e.g., using a measuring tape (Marcus Rowcliffe et al., 2011) or an ultrasonic distance sensor such the Vertex IV system of Haglöf Sweden AB (Henrich et al., 2021).

Obviously, the visual estimation by reference images relies heavily on the operator’s capabilities to estimate the position and distance of an observed animal just by comparing its visual appearance in the field image with the reference images. While some animal locations can be quite reliably estimated (e.g., when the animal is positioned between two trees with known distance), other locations are more difficult to estimate (e.g. when the animal is located in high grass and its position on the ground is not visible). Therefore, the visual estimation by reference images is not only very laborious but also subjective. The on-site distance measurement is slightly less subjective but even more laborious since the location of the camera trap has to be visited in person to obtain measurements for each animal observation.

Camera traps including depth estimation are currently not widely deployed but subject of growing interest in wildlife monitoring and research (Haucke and Steinhage, 2021).

1.2. Contributions

Automating the estimation of camera-to-animal distances from monocular camera images within CTDS demands for two procedures: (1) automated calibration of the observed transect using reference images and measurements, (2) automated estimation of camera-to-animal distances in camera trap images showing observed animals. Figure 1 depicts in the upper area the calibration procedure and in the lower area the distance estimation procedure.

The **calibration procedure** starts with annotated reference images of the transect. The annotation of a reference image depicts the exact distance between the camera and a visible

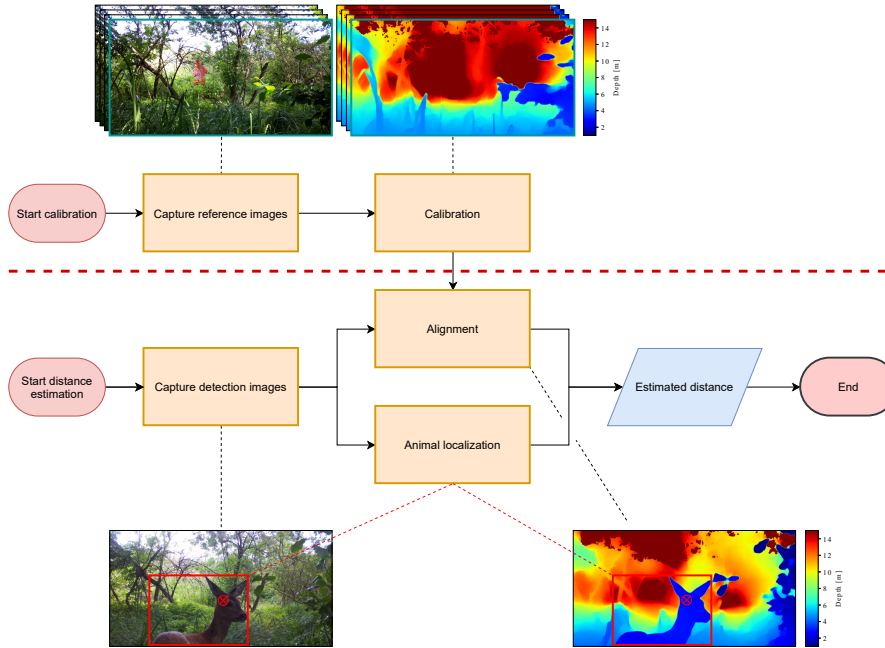


Figure 1.: The overall workflow depicts in the upper area the calibration procedure that derives the calibrated target depth image (highlighted in blue) of the observed transect based on a number N of reference images showing landmarks placed in different distances. This calibration procedure is explained and visualized in more detail in section 3.1 and fig. 2, respectively. The lower area depicts the distance estimation procedure that estimates the real distance of an observed animal based on the localization of the animal in the observation image and an adjustment by the calibrated depth image of the transect. The distance estimation procedure is explained and visualized in more detail in section 3.2.2 and fig. 6, respectively.

landmark (i.e., a distinct object placed on the transect with just the exact distance to the camera). Generally, several reference images are captured with landmarks placed at different distances, e.g., from 1 to 12 m. The calibration procedure generates from these given annotated reference images of a transect a calibrated depth image of the transect with exact distance measurements given in meters. These calibrated depth images are visualized as heatmaps where the distance is lowest in blue and highest in red. This calibration procedure is explained in more detail in section 3.1.

The **distance estimation procedure** starts with a so-called observation image, i.e., an image showing an animal observed in the transect. Using the calibrated depth image of the transect (delivered by the calibration procedure), an exact estimation of the camera-animal distance in meters is derived. This distance estimation procedure is explained in more detail in section 3.2.

2. Data Material

The data for this study was collected by J.H. and H.S.K. in the conservation area ‘Hintenteiche bei Biesenbrow’ located in the Biosphere Reserve Schorfheide-Chorin. The data material is

comprised of intensity images from 24 transects. Intensity images are either RGB (red, green, blue) color images (captured at daytime) or greyscale infrared images (captured at nighttime). For each transect, a sequence of N reference intensity images $\mathbf{I}_i^{\text{ref}}$, with $i \in \{1, 2, \dots, N\}$ is given. Every such image shows a landmark with a known distance to the camera, in distances of 1 meter, 2 meters, ..., N meters. The landmarks of the given dataset are established by a person showing a paper sheet depicting the distance to the camera by the number of meters. Figure 2 depicts two reference images with the researcher and the paper sheet positioned at a distance of 3 meters and 15 meters with respect to the camera, respectively.



Figure 2.: Examples of two reference images with the researcher and the paper sheet acting as a landmark positioned in a distance of 3 meters and 15 meters with respect to the camera, respectively. Each landmark is manually annotated with a binary mask, highlighted in red color. The binary masks of two or more landmarks together with the corresponding uncalibrated disparity images are used to calibrate the target reference depth image, as described in section 3.1.

Table 1 shows the distribution of reference and observation images with respect to the transects.

| | | | | | | | | | | | | |
|---------------|------|------|-----|------|-----|------|------|------|-----|-----|------|-----|
| Transect | T01 | T02 | T05 | T06 | T08 | T09 | T10 | T13 | T14 | T15 | T16 | T17 |
| # Ref. Images | 7 | 7 | 11 | 14 | 12 | 13 | 4 | 9 | 10 | 10 | 5 | 5 |
| # Obs. Images | 4589 | 5753 | 920 | 925 | 942 | 1220 | 3246 | 1949 | 769 | 886 | 140 | 59 |
| Transect | T18 | T19 | T20 | T21 | T22 | T23 | T24 | T25 | T26 | T27 | T28 | T30 |
| # Ref. Images | 12 | 15 | 6 | 6 | 7 | 10 | 10 | 15 | 10 | 7 | 13 | 13 |
| # Obs. Images | 160 | 1111 | 549 | 5135 | 425 | 1210 | 299 | 422 | 332 | 125 | 8356 | 279 |

Table 1.: Distribution of reference and observation images over all 24 transects. The total number of observation images is 39801. Reference images are used to determine the scale of the transect and observation images depict the animals to which the distance should be estimated.

3. Methods

The challenge to overcome the distance estimation bottleneck in CTDS with simple monocular cameras (one camera only instead of two like in stereo vision systems), is the derivation of

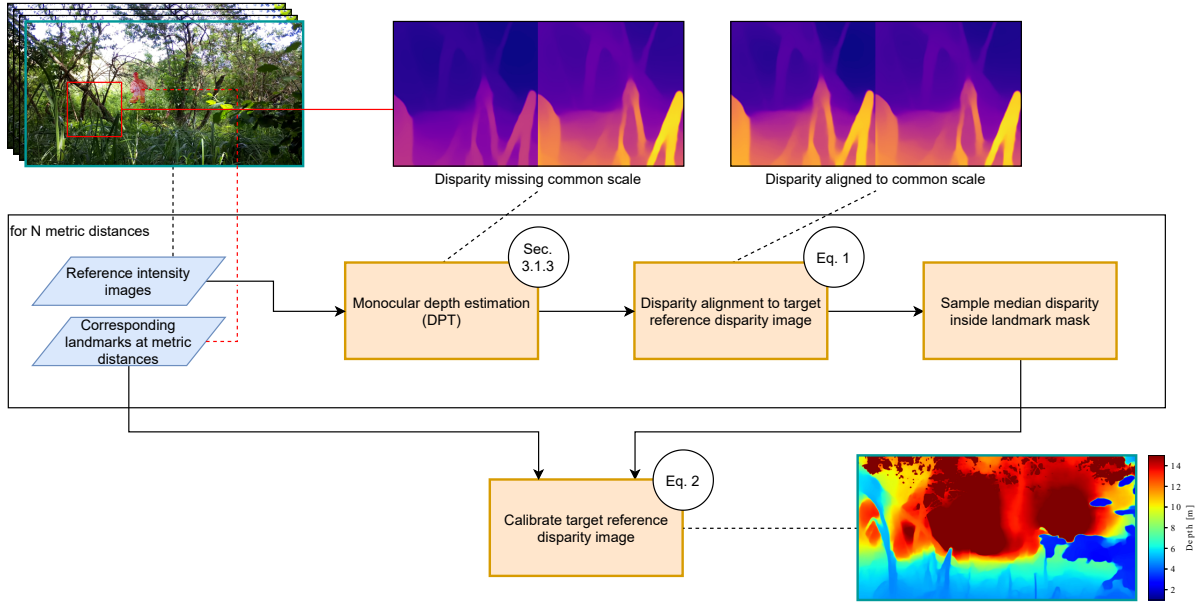


Figure 3.: Calibration workflow which is processed once per transect. The N reference intensity images are used to estimate N corresponding uncalibrated disparity images, as described in section 3.1.1. These uncalibrated disparity images (top-center image pair) are then aligned to a common scale (top-right image pair, c.f. equation 1). The median disparity value inside each landmark binary mask is used together with the known metric landmark distances to calibrate the single target reference disparity image (highlighted in blue, c.f. equation 2). The target reference image is the reference image with the largest landmark distance.

precise distance estimations to objects in the observed scene from just one single image. While distance estimation of a scene from a single image is an easy task for humans by exploiting the scale relative to known objects, perspective, lighting, occlusions, etc., this so-called monocular depth estimation (MDE) is hard to derive for computational models with high accuracy results and low resource requirements.

However, recent developments have shown that detailed distance estimations can be derived from a single image in an end-to-end manner based on deep learning approaches (Facil et al., 2019). Meanwhile, various deep learning have shown their effectiveness to address the monocular depth estimation. In this study, we decide for the DPT (Dense Prediction Transformers) approach that has shown superior quantitative and qualitative results in MDE also due to a training procedure based on a wide variety of multiple complementary sources (Ranftl et al., 2021).

3.1. Camera Trap Calibration

Calibration of a camera trap employs reference images that depict landmarks of known distances to the camera. It is important to note that the reference images may be acquired in a multitude of ways since our calibration method is agnostic to the exact generation of the reference images. In this study, the landmarks are established by a person showing a paper sheet depicting the distance to the camera by the number of meters (cf. fig. 2).

3.1.1. Uncalibrated depth images via monocular depth estimation

For each camera trap, there are N reference images $\mathbf{I}_i^{\text{ref}}$ with a corresponding binary mask $\mathbf{M}_i^{\text{ref}}$ covering the landmark (depicted red in fig. 2) and the corresponding true distance z_i between camera and landmark for $i \in \{1, \dots, N\}$. We refer to the N -th reference image as the *target reference image*. The N reference images $\mathbf{I}_i^{\text{ref}}$ are first propagated through the DPT (Ranftl et al., 2021) depth estimation model which results in N uncalibrated disparity images $\mathbf{D}_i^{\text{ref}}$ depicting the pixel-wise inverse distances to scene objects in a relative way, i.e., depth image pixels in blue are closer than those in green that in turn are closer than those in yellow which in turn are closer than those in red. More precisely: the uncalibrated disparity images show inverse distance estimations up to an unknown scale parameter m and an unknown shift parameter c .

3.1.2. Calibrated depth images via RANSAC

Therefore, at least two landmarks with known distances to the camera must be used to determine both parameters. In this dataset, each of the N reference images $\mathbf{I}_i^{\text{ref}}$ depicts exactly one landmark, i.e., the researcher with a paper sheet. Since the landmarks are distributed over all N reference images $\mathbf{I}_i^{\text{ref}}$, prior to the metric calibration, we align all uncalibrated disparity images to one common, yet not calibrated, scale. To be precise, for each uncalibrated disparity image $\mathbf{D}_i^{\text{ref}}$ with $i \in \{1, \dots, N - 1\}$, we estimate two parameters m_i^*, c_i^* , using the RANSAC approach (Fischler and Bolles, 1981), such that

$$(m_i^*, c_i^*) \approx \arg \min_{m_i, c_i} \sum_{i=1}^{N-1} |m_i \cdot \mathbf{D}_i^{\text{ref}}(\mathbf{M}_i^{\text{ref}} = 0) + c_i - \mathbf{D}_N^{\text{ref}}(\mathbf{M}_N^{\text{ref}} = 0)|, \quad (1)$$

where $\mathbf{D}_i^{\text{ref}}(\mathbf{M}_i^{\text{ref}} = 0)$ depicts all pixels in the disparity image $\mathbf{D}_i^{\text{ref}}$ outside the binary mask $\mathbf{M}_i^{\text{ref}}$ covering the landmark, i. e., all pixels depicting the visible stationary components of the observed scene. This alignment ensures the optimal alignment of all landmarks used in the next calibration step. Given the N landmarks in the aligned uncalibrated disparity images $\mathbf{D}_i^{\text{ref}}$ with $i \in \{1, \dots, N - 1\}$, the RANSAC approach (Fischler and Bolles, 1981) is then used to estimate the unknown scale parameter m and the unknown shift parameter c with the objective of minimizing the absolute disparity error:

$$(m^*, c^*) \approx \arg \min_{m, c} \sum_{i=1}^N |m \cdot \text{median} \left(m_i^* \cdot \mathbf{D}_i^{\text{ref}}(\mathbf{M}_i^{\text{ref}} = 1) + c_i^* \right) + c - \frac{1}{z_i}|, \quad (2)$$

where $\mathbf{D}_i^{\text{ref}}(\mathbf{M}_i^{\text{ref}} = 1)$ depicts all pixels in the disparity image $\mathbf{D}_i^{\text{ref}}$ within the binary mask $\mathbf{M}_i^{\text{ref}}$ covering the landmark. From these disparity values the median value is chosen for minimization due to the improved robustness when facing imperfect landmark masks compared to the mean. The real metric distance to the respective landmark (i.e., the ground truth) is depicted with z_i , the shift and scale parameters of disparity image $\mathbf{D}_N^{\text{ref}}$ are given as $m_N^* = 1$ and $c_N^* = 0$. The resulting calibrated disparity images $\mathbf{C}_i^{\text{ref}}$ and metric depth images $\mathbf{Z}_i^{\text{ref}}$ are then given by equations 3 and 4, respectively:

$$\mathbf{C}_i^{\text{ref}} = m^* \cdot \mathbf{D}_i^{\text{ref}} + c^*, \quad (3)$$

$$\mathbf{Z}_N^{\text{ref}} = (\mathbf{C}_N^{\text{ref}})^{-1}. \quad (4)$$



Figure 4.: Workflow which is applied on each animal observation image. From the intensity image, we estimate an uncalibrated disparity image, as described in section 3.2.1. We subsequently calibrate the observation depth image by aligning the depth to the target reference depth image (c.f. section 5). We then sample the 20th percentile of the calibrated depth inside each detected animal bounding box to produce a single depth estimation for each animal (c.f. section 3.2.2).

Instead of metric distances with image values in $[0, \infty]$ we can deal with disparity values in $[0, w]$ where w is the image width. This results in improved numerical stability and induces lower weighting of more distant landmarks, reflecting the lower accuracy of the depth estimation at large distances. We refer to $\mathbf{C}_N^{\text{ref}}$ and $\mathbf{Z}_N^{\text{ref}}$ as the *target* reference disparity and depth images, respectively. This target reference depth image is highlighted in blue in figure 1.

3.2. Animal Distance Estimation

For each detected animal observation, we have to estimate a single metric distance to the animal. This objective demands to solve two requirements: (1) deriving a calibrated depth image \mathbf{Z}^{obs} of the camera trap image \mathbf{I}^{obs} depicting the observed animal, (2) localization of the observed animal in this calibrated depth image \mathbf{Z}^{obs} .

3.2.1. Deriving a calibrated depth image for each animal observation

Sampling accurate distance information for each observation image \mathbf{I}^{obs} employs the scale information of the calibration step described in section 3.1. We achieve this by transferring the scale of the calibrated reference disparity images $\mathbf{C}_i^{\text{ref}}$ to the estimated disparity images \mathbf{D}^{obs} of each animal observation. One might think that a simpler approach would be to just sample the depth of the calibrated reference images. However, the scenes observed by the camera traps are highly dynamic (due to trees falling over, plants gaining or losing leaves, etc.), leading to higher estimation errors when employing this strategy. Therefore, we employ again the monocular depth estimation by DPT Ranftl et al. (2021) to estimate first an uncalibrated disparity image \mathbf{D}^{obs} of each observation image \mathbf{I}^{obs} . We then transfer the metric scale acquired

during calibration onto the uncalibrated disparity of each observation \mathbf{D}^{obs} . From all possible N calibrated reference disparity images $\mathbf{C}_i^{\text{ref}}, i \in \{1, \dots, N\}$ to inform this metric scale we use the calibrated target reference disparity $\mathbf{C}_N^{\text{ref}}$, i.e., the one representing the calibration landmark with the largest distance. This choice shows the minimum number of pixels depicting the calibration landmark and therefore the maximum number of image pixels with an associated depth value that depict the scene where the animal is observed. We transfer the scale of the target depth image to the uncalibrated observation disparity image by again estimating the scale and shift parameters m and c using RANSAC (Fischler and Bolles, 1981) while minimizing the absolute disparity error over the entire images, while excluding the calibration landmark and bounding boxes of detected animals (c.f. section 3.2.2):

$$(m^*, c^*) \approx \arg \min_{m, c} |m \cdot \mathbf{C}_N^{\text{ref}}(\mathbf{M}_N^{\text{ref}} = 0) + c - \mathbf{D}_N^{\text{obs}}(\mathbf{M}_N^{\text{obs}} = 0)| \quad (5)$$

Analogous to equation 4, the result is the calibrated depth observation image \mathbf{Z}^{obs} of the observation image \mathbf{I}^{obs} .

3.2.2. Localization of the observed animal in this calibrated depth image

For animal detection we apply the MegaDetector animal detection model (Beery et al., 2019) to the observation image \mathbf{I}^{obs} , resulting in a bounding box for each animal observed in \mathbf{I}^{obs} . From all detected bounding boxes corresponding to a single observation, we infer a binary mask \mathbf{M}^{obs} which is set to one at each pixel inside any detected bounding box and to zero everywhere else. This binary mask is used in equation 5. Then, we sample for each bounding the 20th percentile of the corresponding calibrated depth observation image \mathbf{Z}^{obs} . This procedure is simple but effective. It is also intuitive, as the animals are mostly positioned on a much more distant background and slightly occluded by plants or trees. The 20th percentile of the depth then presents an accurate estimate of the true distance, as illustrated by figure 5. We also evaluated more sophisticated methods for precise localization such as class attention maps (CAMs, Zhou et al. (2016)) of species classification models (Microsoft Corporation, 2019) but found these models to fail in many instances when the animals are strongly occluded. The classification of animals is therefore performed by a human observer and not automated.

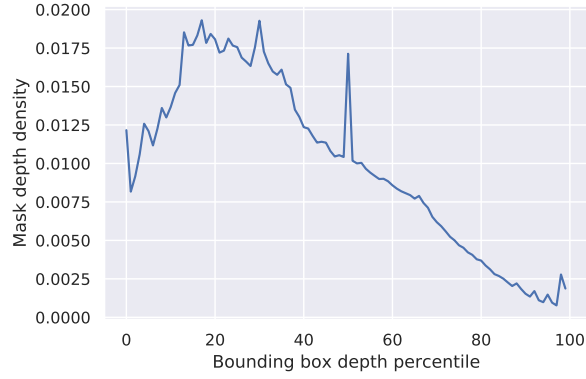


Figure 5.: Average density of depth inside manually annotated masks of 100 randomly sampled observations over the percentiles of depth values inside the enclosing bounding boxes. When sampling roughly at the 20th percentile of the depth contained inside the detected bounding boxes, the probability is maximal that the sampled depth is inside the manually annotated mask and therefore lies directly on the detected animal.

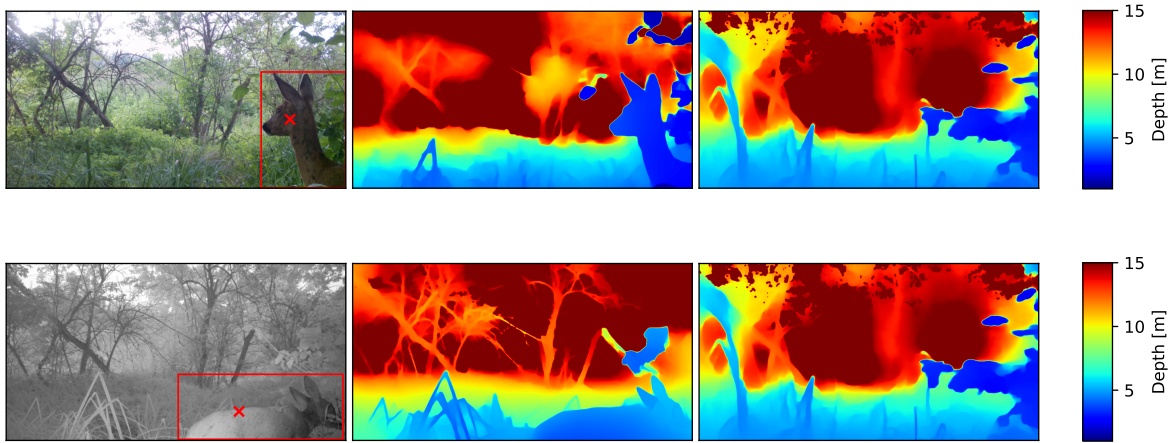


Figure 6.: Examples of a calibrated animal observation image. Left: Color (daytime) or infrared (nighttime) observation images with a bounding box and the resulting distance sampling location via the 20th percentile. Center: The corresponding estimated and calibrated depth image. Right: The target reference depth image corresponding to the calibration landmark with the largest distance. As can be observed, the background changes slightly between both images. This is due to the fact that both images were captured with a difference in time of two months.

3.2.3. Distance Correction

When employing manual distance estimation, equal reference depths are assumed to be located at a straight horizontal line orthogonal to the optical axis. In reality however, equal reference

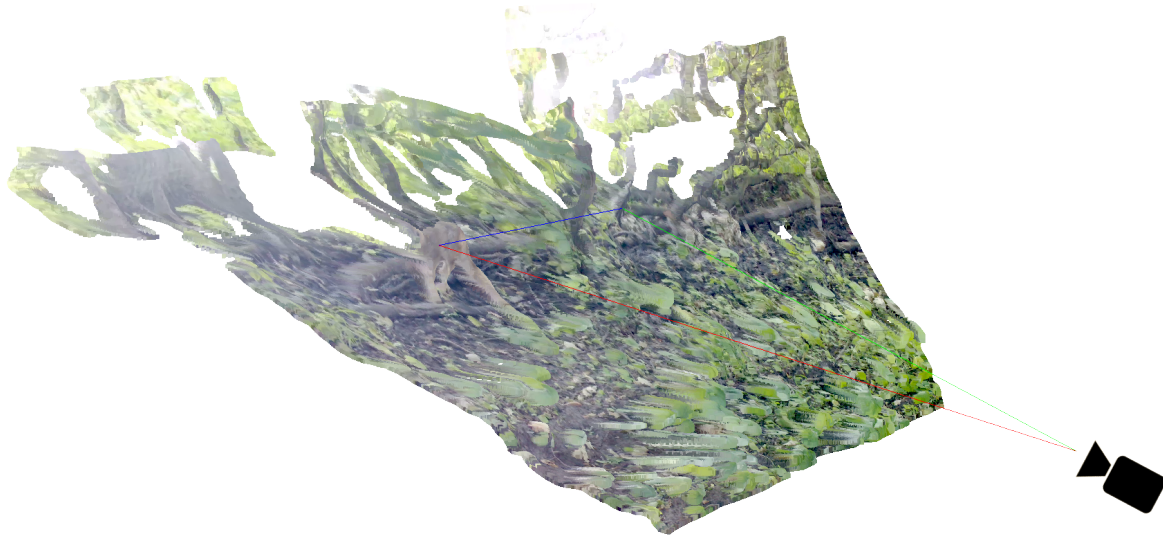


Figure 7.: Geometry of the distance correction with a 3D scene reconstruction. The camera is located on the bottom right, the animal (a deer calf) is located in the top left. The line from the camera's optical center to the location of the animal (red) forms the angle α with the optical axis. In manual distance sampling, the animal's distance is estimated according to reference landmarks lying on the horizontal line orthogonal to the optical axis (blue), resulting in the distance estimation depicted in green. As can be seen, the manually estimated distance g and the true distance d differs more strongly with a larger angle α .

depths are located on a circle segment with the camera at the center and the radius d . This is also the distance which is measured by our method. Figure 7 illustrates the corresponding geometry. The relation between both distances is given by:

$$d = \frac{g}{\cos \alpha}$$

We therefore correct our distance estimation by multiplying it with $\cos \alpha$ to be compatible with the employed ground truth.

3.2.4. Metrics

For evaluation, we employ the mean absolute distance estimation error over all observations $m \in \{1, \dots, M\}$, defined as:

$$\frac{1}{M} \sum_{m=1}^M |z_m^{\text{est}} - z_m^{\text{gt}}| \quad (6)$$

and the mean distance estimation error in our evaluation, defined as:

$$\frac{1}{M} \sum_{m=1}^M z_m^{\text{est}} - z_m^{\text{gt}} \quad (7)$$

where z_m^{est} and z_m^{gt} represent the estimated and ground-truth distance of each observation, respectively.

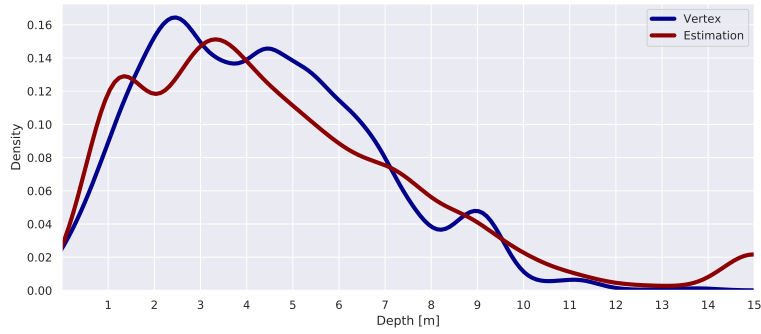


Figure 8.: Probability density of the ground truth and estimated distances. As can be seen, the distribution of estimated distances closely matches the ground truth distance distribution.

4. Evaluation and Discussion

For the resulting distance estimations to be usable for camera trap distance sampling, it is important that our estimation method produces a distance distribution as close to the ground truth and as unbiased as possible. As can be seen in figure 8, the distribution of estimated distances indeed reflects the ground truth distribution. At 2m both distributions differ by about 4 percentage points while the difference at 9m is about 1 percentage point. We achieve a mean distance error of 0.10 m and a mean absolute distance error of 1.85 m. The small positive bias of our method can be explained by the distribution of distance values in the calibrated depth images. Large parts of the depth images show background areas with arbitrarily large distances. If an animal is falsely detected in such an area, a very large distance is falsely estimated. Both the mean and the mean absolute distance error measures depend strongly on the transect, as can be seen in figure 9. High estimation errors can be observed with dense vegetation directly in front of the camera (e.g., T24), as the employed monocular depth estimation tends to smooth out the estimated disparity images, which is especially damaging for small cavities in the vegetation, in which the background then appears closer than it truly is. In this case, the initial calibration (c.f. section 3.1) fails because the known landmarks appear to be in a single plane. In other transects (e.g., T02), the forest ground is only visible to a small degree. This apparently also reduces monocular depth estimation accuracy because important context information about the relative location of objects in the scene is lost.

4.1. Camera Trap Setup Guidelines

The choice of scene and the camera setup is therefore an important factor for the success of our method. A calibration result of a well-conditioned setup can be seen in figure 10. We want to provide researchers with guidelines on where and how to best place camera traps in the future to make the best use of our method and therefore make the following recommendations:

- Camera traps should be tightly secured to stationary objects, i.e. trees. This reduces camera motion and hence ensures a strong overlap of observation images with reference images

- the field of view of the camera trap should be free of vegetation inside a radius of three meters to reduce the number of observations in small gaps of such vegetation
- at least the bottom third of the image produced by the camera trap should be covered by the ground to ensure enough context information for the monocular depth estimation
- if possible, in the future, fixed reference objects should be placed and stay in the scene so that accurate calibration can be performed separately for each observation, without the now required reference images

The original dataset contains five additional transects (T03, T04, T07, T11, T12) which do not satisfy multiple of the above recommendations, which led to clearly suboptimal results. Hence, we did not include these transects in our evaluation.

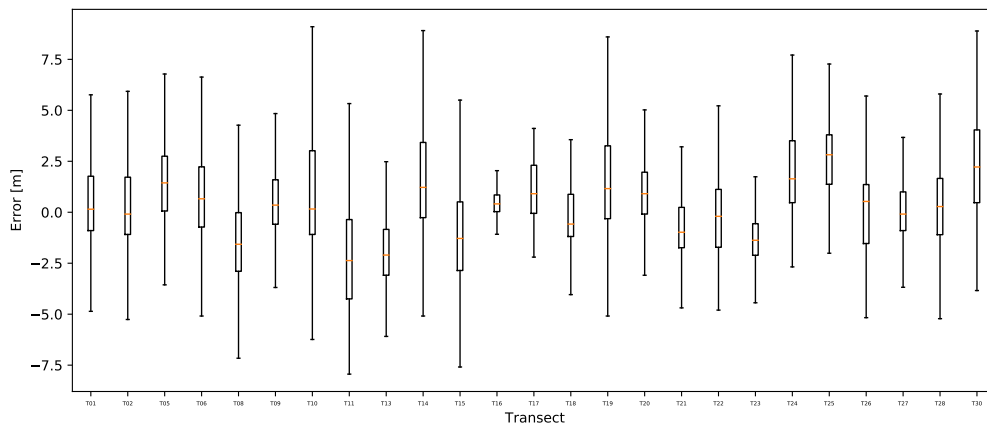


Figure 9.: Box plot of the distance estimation error per transect.

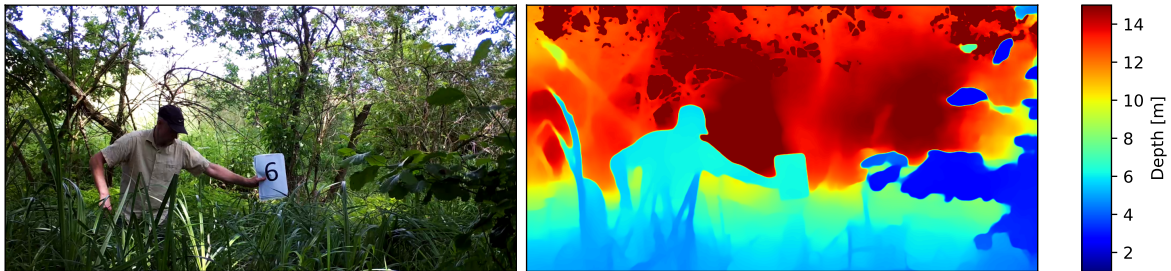


Figure 10.: Exemplary reference image of transect T06. Left: Color (daytime) reference image. Right: The corresponding calibrated reference depth image obtained as described in section 3.1.

4.2. User Study

To quantify the reduction of the manual distance estimation workload facilitated by our method, we conducted a user study with five users experienced with wildlife monitoring using

camera trap imagery. Out of the data described in table 1, we randomly chose five transects, out of which we randomly sampled five detection videos with no more than one single animal present at a time. The participants of the study are then asked to apply the manual distance estimation process (cf. appendix A). We chose only observations with at most a single animal present at a time to prevent ambiguous assignments between multiple individuals over the participants and to therefore be able to quantify the deviation of distance estimations between participants. The time needed by a participant to compare the position of an observed animal in a video frame to the different distances in the reference video clips and estimate the distance has been measured to lie between 8.6s and 17.9s. The mean time needed per observation is 12s. Extrapolated to the complete dataset described in table 1, this would result in a total effort of about 130 person hours. This is however a lower bound, as we sampled only observations with at most a single animal, which reduces the time needed compared to observations with multiple animals. In comparison, our method requires a manual annotation effort of about 6 person hours and a runtime of 24h. Our method therefore reduces the manual effort by a factor of ~ 22 and the total runtime by a factor of ~ 5 . We also compared the quality of the manual distance estimations produced by the participants. In 9% of cases, the participants disagree on whether an animal is visible in the image. The mean standard deviation between the participants over the remaining 91% of measurements is 62 cm, suggesting a lower bound of the achievable accuracy.

5. Conclusion

Camera trap distance sampling (CTDS) is a survey method to estimate animal abundance across a wide range of taxa from a limited set of locations (transects). However, CTDS entails a distance estimation bottleneck, i.e., CTDS requires the distances from camera traps to the observed animals. We successfully overcome the distance estimation bottleneck for CTDS by employing monocular depth estimation and developing a robust calibration method for uncalibrated depth images. Our automated method achieves a mean distance error of only 0.14 m and it reduces the manual effort by a factor larger than 18 and the total runtime by a factor of 4. Our method imposes no constraints on specific camera hardware and is therefore applicable to a wide variety of datasets. In our experiments, we succeed in closely matching the true distance distribution, which facilitates large-scale automated distance sampling. Future work could improve the temporal stability of monocular depth estimation and in turn further improve the distance estimation accuracy. In cases where image sequences are available for each animal observation, multi-object tracking approaches would likely reduce false positive and false negative observations.

Acknowledgments

This research has been funded in part by the Federal Ministry of Education and Research (www.bmbf.de) of the Federal Republic of Germany under grant number 01DK17048. We would like to thank the Helversen'sche Stiftung for providing permission and access to the FFH conservation area 'Hintenteiche bei Biesenbrow' and are grateful for support of our work by Dorothea Dietrich, Dietmar Nill, Ulrich Stöcker and Thomas Volpers. We would also like to thank Dr. Martin Flade and Rüdiger Michels from the Biosphere Reserve Schorfheide-Chorin.

Appendices

A. Manual Distance Estimation Process

Result: Manual distance estimations

open a spreadsheet

foreach *transect* **do**

 note the transect and starting time in the spreadsheet

foreach *observation video in transect* **do**

 open the respective video file

foreach *video runtime from 0 to 58 s in 2 s steps* **do**

 pause the video

 locate the animal

if *an animal is present* **then**

 compare the position of the animal to the different distances in the
 reference images

 estimate the most accurate lower integer distance bound and note it in
 the spreadsheet

else

 note that no animal is present

end

end

end

 note the elapsed time in the spreadsheet

end

Algorithm 1: Description of the manual distance estimation process which we employed

References

- Sara Beery, Dan Morris, and Siyu Yang. Efficient pipeline for camera trap image review. *arXiv preprint arXiv:1907.06772*, 2019.
- Mattia Bessone, Hjalmar S. Kühl, Gottfried Hohmann, Ilka Herbinger, Kouame Paul N’Goran, Papy Asanzi, Pedro B. Da Costa, Violette Dérozier, Ernest D. B. Fotsing, Bernard Ikembelo Beka, Mpongo D. Iyomi, Iyomi B. Iyatshi, Pierre Kafando, Mbangi A. Kambere, Dissondet B. Moundzoho, Musubaho L. K. Wanzalire, and Barbara Fruth. Drawn out of the shadows: Surveying secretive forest species with camera trap distance sampling. *Journal of Applied Ecology*, 57(5):963–974, 2020. doi: <https://doi.org/10.1111/1365-2664.13602>. URL <https://besjournals.onlinelibrary.wiley.com/doi/abs/10.1111/1365-2664.13602>.
- Noémie Cappelle, Marie-Lyne Després-Einspenner, Eric J. Howe, Christophe Boesch, and Hjalmar S. Kühl. Validating camera trap distance sampling for chimpanzees. *American Journal of Primatology*, 81(3):e22962, 2019. doi: <https://doi.org/10.1002/ajp.22962>. URL <https://onlinelibrary.wiley.com/doi/abs/10.1002/ajp.22962>.
- Luca Corlatti, Stefano Sivieri, Bogna Sudolska, Stefano Giacomelli, and Luca Pedrotti. A field test of unconventional camera trap distance sampling to estimate abundance of marmot populations. *Wildlife Biology*, 2020(4), 2020.
- J. Facil, B. Ummenhofer, H. Zhou, L. Montesano, T. Brox, and J. Civera. Cam-convs: Camera-aware multi-scale convolutions for single-view depth. In *IEEE International Conference on Computer Vision and Pattern Recognition (CVPR)*, 2019. URL <http://lmb.informatik.uni-freiburg.de/Publications/2019/ZUB19>.
- Martin A Fischler and Robert C Bolles. Random sample consensus: a paradigm for model fitting with applications to image analysis and automated cartography. *Communications of the ACM*, 24(6):381–395, 1981.
- Haglöf Sweden AB. Vertex iv. <https://web.archive.org/web/20210121013130/http://www.haglofcg.com/index.php/en/products/instruments/height/341-vertex-iv>. Accessed: 2021-01-21.
- Timm Haucke and Volker Steinhage. Exploiting depth information for wildlife monitoring, 2021.
- Maik Henrich, Marco Heurig, and Christian Fiderer. Distance measurement in wildlife monitoring using ultrasonic distance sensors. Faculty of Environment and Natural Resources, Univ. of Freiburg, 2021. Personal communication.
- Eric J. Howe, Stephen T. Buckland, Marie-Lyne Després-Einspenner, and Hjalmar S. Kühl. Distance sampling with camera traps. *Methods in Ecology and Evolution*, 8(11):1558–1565, 2017. doi: [10.1111/2041-210X.12790](https://doi.org/10.1111/2041-210X.12790). URL <https://besjournals.onlinelibrary.wiley.com/doi/abs/10.1111/2041-210X.12790>.
- J Marcus Rowcliffe, Chris Carbone, Patrick A Jansen, Roland Kays, and Bart Kranstauber. Quantifying the sensitivity of camera traps: an adapted distance sampling approach. *Methods in Ecology and Evolution*, 2(5):464–476, 2011.

Microsoft Corporation. Ai for earth species classification. <https://github.com/microsoft/SpeciesClassification>, 2019. Accessed: 2021-02-18.

René Ranftl, Alexey Bochkovskiy, and Vladlen Koltun. Vision transformers for dense prediction. *arXiv preprint arXiv:2103.13413*, 2021.

Bolei Zhou, Aditya Khosla, Agata Lapedriza, Aude Oliva, and Antonio Torralba. Learning deep features for discriminative localization. In *Proceedings of the IEEE conference on computer vision and pattern recognition*, pages 2921–2929, 2016.